Drug Design, Development and Therapy

Dovepress
open access to scientific and medical research

Open Access Full Text Article

ORIGINAL RESEARCH

Potent human uric acid transporter 1 inhibitors: in vitro and in vivo metabolism and pharmacokinetic studies

This article was published in the following Dove Press journal:
Drug Design, Development and Therapy
7 November 2012
Number of times this article has been viewed

Michael F Wempe[1]
Janet W Lightner[2]
Bettina Miller[1]
Timothy J Iwen[1]
Peter J Rice[1]
Shin Wakui[3]
Naohiko Anzai[4]
Promsuk Jutabha[4]
Hitoshi Endou[5]

[1]Department of Pharmaceutical Sciences, School of Pharmacy, University of Colorado Denver, Anschutz Medical Campus, Aurora, CO, USA; [2]Department of Pharmacology, East Tennessee State University, Johnson City, TN, USA; [3]Department of Toxicology, Azabu University School of Veterinary Medicine, Chuo Sagamihara, Kanagawa, Japan; [4]Department of Pharmacology and Toxicology, Dokkyo Medical University School of Medicine, Mibu, Shimotsuga, Tochigi, Japan; [5]Department of Pharmacology and Toxicology, Kyorin University School of Medicine, Mitaka, Tokyo, Japan

Abstract: Human uric acid transporter 1 (hURAT1; SLC22A12) is a very important urate anion exchanger. Elevated urate levels are known to play a pivotal role in cardiovascular diseases, chronic renal disease, diabetes, and hypertension. Therefore, the development of potent uric acid transport inhibitors may lead to novel therapeutic agents to combat these human diseases. The current study investigates small molecular weight compounds and their ability to inhibit ^{14}C-urate uptake in oocytes expressing hURAT1. Using the most promising drug candidates generated from our structure–activity relationship findings, we subsequently conducted in vitro hepatic metabolism and pharmacokinetic (PK) studies in male Sprague-Dawley rats. Compounds were incubated with rat liver microsomes containing cofactors nicotinamide adenine dinucleotide phosphate and uridine 5′-diphosphoglucuronic acid. In vitro metabolism and PK samples were analyzed using liquid chromatography/mass spectrometry-mass spectrometry methods. Independently, six different inhibitors were orally (capsule dosing) or intravenously (orbital sinus) administered to fasting male Sprague-Dawley rats. Blood samples were collected and analyzed; these data were used to compare in vitro and in vivo metabolism and to compute noncompartmental model PK values. Mono-oxidation (Phase I) and glucuronidation (Phase II) pathways were observed in vitro and in vivo. The in vitro data were used to compute hepatic intrinsic clearance, and the in vivo data were used to compute peak blood concentration, time after administration to achieve peak blood concentration, area under the curve, and orally absorbed fraction. The experimental data provide additional insight into the hURAT1 inhibitor structure–activity relationship and in vitro–in vivo correlation. Furthermore, the results illustrate that one may successfully prepare potent inhibitors that exhibit moderate to good oral bioavailability.

Keywords: benzbromarone analogs, bioavailability, glucuronidation, oxidation, structure–activity relationship

Introduction

It is well known that humans metabolize purine nucleotides to produce uric acid (urate) and that we eliminate uric acid mainly via the kidneys. Clearly a function of diet, age, and overall health, studies have illustrated that normal adults excrete roughly 500–600 mg of urate per day.[1,2] In 2002, Enomoto et al[3] first published research identifying human uric acid transporter 1 (hURAT1; SLC22A12), a transporter protein now recognized as a very important urate anion exchanger functioning to regulate urate blood level. Elevated urate levels are believed to play a pivotal role in cardiovascular diseases, chronic renal disease, diabetes, and hypertension.[4–9] We believe that designing potent uric acid transporter inhibitors may lead to novel therapeutic agents. Our previous works have described chemical synthesis and in vitro testing that produced

Correspondence: Michael F Wempe
Department of Pharmaceutical Sciences, School of Pharmacy, University of Colorado Denver, Anschutz Medical Campus, C238; 12850 E Montview Blvd, Aurora, CO 80045, USA
Tel +1 303 724 8982
Fax +1 303 724 7266
Email michael.wempe@ucdenver.edu

important hURAT1 structure–activity relationship (SAR) data.[10,11] As illustrated in Figure 1, we probed three different benzofuran templates (I, II, and III) and their ability to inhibit ^{14}C-urate uptake in oocytes expressing hURAT1. Our previous work provided important insights regarding required chemical features; in summary, the data supported the notion that an anion (preferably on the C-ring; Figure 1) is required in order to interact with a positively charged hURAT1 binding pocket.[10,11] The previous studies also demonstrated how electronic donating and/or withdrawing groups attached to the B-ring influence inhibitory potency. As depicted in Table 1, the current study investigates the three constitutional isomer templates. Compounds (1)–(19), (20)–(22), and (23)–(26) represent template I, II, and III examples, respectively. The current work includes: (1) efforts to address a few unanswered SAR questions; (2) performing in vitro metabolism experiments to generate in vitro hepatic intrinsic clearance (CL_{int}) data, and using the in vitro data to pick lead molecules; and (3) examining the promising drug candidates by conducting in vivo pharmacokinetic (PK) studies in male Sprague-Dawley rats and subsequently generating noncompartmental model PK parameters such as peak blood concentration (C_{max}), time after administration to achieve peak blood concentration (T_{max}), half-life ($T_{1/2}$), area under the curve ($AUC_{0-\infty}$), and orally absorbed fraction (F_a).

Materials and methods

Chemicals and equipment

Alamethicin, ammonium chloride (NH_4Cl), anhydrous sodium sulfate (Na_2SO_4), *p*-anisoyl chloride, benzoyl chloride-d_5, carboxy-methyl cellulose sodium (CMC), carbon disulfide (CS_2), 3,5-dichloro-4-hydroxybenzoic acid, 3,5-dimethyl-4-methoxy-benzoic acid, 3,5-di-tert-butyl-4-hydroxybenzoic acid, deuterated chloroform ($CDCl_3$), dimethyl sulfoxide (DMSO), ethylenediaminetetraacetic acid (EDTA), formic acid, iodomethane, 3-iodo-4-methoxybenzoic acid, magnesium chloride ($MgCl_2$), *N*-bromosuccinimide (NBS), nicotinamide adenine dinucleotide phosphate (NADPH), sodium ethanethiolate (NaSEt), thionyl chloride ($SOCl_2$), tin (IV) chloride, UDP-glucuronic acid (UDPGA), and verapamil hydrochloride were purchased from Sigma-Aldrich (St Louis, MO). Acetic acid (AA), benzene, concentrated hydrochloric acid (HCl), dimethylformamide (DMF), ethyl acetate (EtOAc), hexanes (Hex), high-performance liquid chromatography (HPLC) grade methanol (MeOH), HPLC grade acetonitrile (ACN), tetrahydrofuran (THF), HPLC grade water (H_2O), isopropanol, methylene chloride (DCM), potassium carbonate (K_2CO_3), sodium bicarbonate ($NaHCO_3$), sodium chloride (NaCl), sodium hydroxide (NaOH), and toluene were purchased from Fisher Scientific (Pittsburgh, PA). 2-Butylbenzofuran was purchased from TCI America (Chicago, IL). Hydroxybutenyl-beta-cyclodextrin (HBenβCD; Batch X29556-164) was a gift from Eastman Chemical Company (Kingsport, TN). Reactions were monitored via silica gel IB2-F thin-layer chromatography (TLC) plates from JT Baker (Phillipsburg, NJ). Sprague-Dawley rat microsomes (liver: Lot No 0510153, pool of 431; intestine: Lot No 0810107, pool of 249) were acquired from Xenotech LLC (Kansas City, KS).

The ^{1}H and ^{13}C nuclear magnetic resonance (NMR) spectra were recorded using a 400 MHz Bruker NMR, Avance III 400 (Fremont, CA). The chemical shifts are reported in ppm. An Applied Biosystems Sciex 4000 (Applied Biosystems, Foster City, CA) was equipped with a Shimadzu HPLC (Shimadzu Scientific Instruments, Inc, Columbia, MD) and a Leap auto-sampler (LEAP Technologies, Carrboro, NC) was used. Liquid chromatography employed an Agilent Technologies, Zorbax extended-C18 50 × 4.6 mm (or 250 × 4.6 mm; metabolite resolution investigations) 5 micron column at 40°C with a flow rate of 0.4 mL/min.

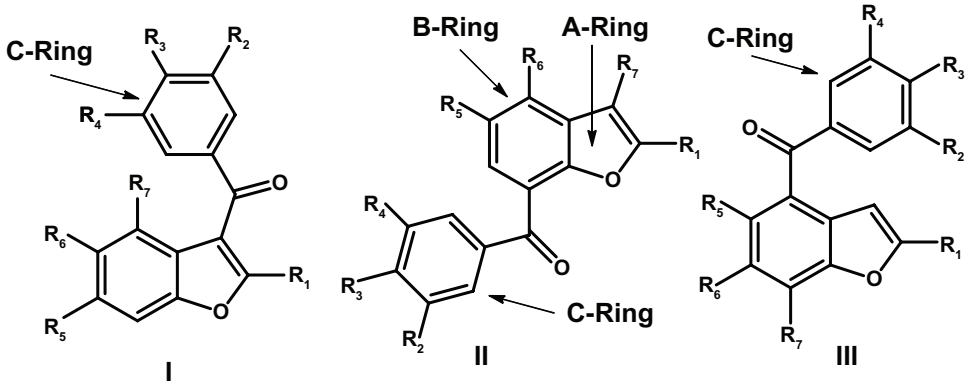

Figure 1 Benzofuran chemical templates I, II, and III.

Table 1 Compound structure and hURAT1 in vitro inhibition data summary

Compound	Template	hURAT1							
		IC_{50}[a] (nM) ± SD	R1	R2	R3	R4	R5	R6	R7
(1)	I	26 ± 3	Et	Br	OH	Br	H	H	H
(2)	I	2460 ± 900	Et	H	OH	H	H	O-Me	H
(3)	I	111 ± 14	Et	Br	OH	Br	O-Me	H	H
(4)	I	1650 ± 120	Et	Br	OH	Br	O-Me	Br	H
(5)	I	138 ± 88	Et	Br	OH	Br	OH	H	H
(6)	I	42 ± 9	Et	Br	OH	Br	H	O-Me	H
(7)	I	23460 ± 270	Et	H	O-Me	H	Br	OH	Br
(8)	I	189 ± 90	Et	Br	OH	Br	H	OH	H
(9)	I	6 ± 4	Et	Br	OH	Br	H	F	H
(10)	I	2410 ± 90	Et	F	OH	H	H	H	H
(11)	I	874 ± 56	Et	Cl	OH	H	H	H	H
(12)	I	814 ± 160	Et	Br	OH	H	H	H	H
(13)	I	1490 ± 80	Et	I	OH	H	H	H	H
(14)	I	ND	Et	t-Bu	OH	t-Bu	H	H	H
(15)	I	7540 ± 60	Et	Me	OH	Me	H	H	H
(16)	I	1219 ± 110	Et	Br	O-Me	Br	H	H	H
(17)	I	ND	Bu	H	OH	H	H	H	H
(18)	I	1932 ± 90	Bu	Br	OH	Br	H	H	H
(19)	I	399 ± 56	Et	Cl	OH	Cl	H	H	H
(20)	II	ND	Et	H	O-Me	H	O-Me	H	H
(21)	II	1440 ± 140	Et	Br	OH	Br	O-Me	H	H
(22)	II	287 ± 118	Et	Br	OH	Br	OH	H	H
(23)	III	772 ± 215	Et	H	O-Me	H	H	Br	OH
(24)	III	358 ± 130	Et	Br	OH	Br	O-Me	H	H
(25)	III	83 ± 10	Et	Br	OH	Br	OH	H	H
(26)	III	177 ± 80	Et	Br	OH	Br	H	Br	OH

Note: [a]$IC_{50} > 25$ μM.
Abbreviations: hURAT1, human uric acid transporter 1; ND, no data; SD, standard deviation.

The mobile phase consisted of A: 10 mM (NH_4OAc), 0.1% formic acid in H_2O, and B: 50:50 ACN:MeOH. Unless denoted otherwise, the chromatography method used was 95% A for 1.0 minute, ramped to 95% B at 3.0 minutes and held for 4.5 minutes, and, lastly, brought back to 95% A at 8.5 minutes and held for 1.0 minute (9.5 minutes total run time). Synthesized compounds were monitored via electro-spray ionization positive ion mode (ESI+) using the following conditions: (1) an ion spray voltage of 5500 V; (2) temperature 450°C; (3) curtain gas (CUR; set at 10) and collisionally activated dissociation (CAD; set at 5) gas was nitrogen; (4) ion source gas one (GS1) and two (GS2) was set at either 20 or 25 and specifically denoted in the individual compound section; (5) entrance potential was set at 10 V; (6) quadruple one (Q1) and three (Q3) were set on unit resolution; (7) dwell time was set at 200 msec; and (8) declustering potential (DP), collision energy (CE), and collision cell exit potential (CXP) are voltages (V). Samples (10 μL) were analyzed by liquid chromatography/mass spectrometry-mass spectrometry (LC/MS-MS). As judged by NMR and LC/MS-MS analysis, all purified compounds were >97% pure.

Chemical synthesis

Synthesis of the following compounds has been described previously: (3,5-dibromo-4-hydroxyphenyl)(2-ethylbenzofuran-3-yl)methanone (1), (2-ethyl-5-methoxybenzofuran-3-yl)(4-hydroxyphenyl)methanone (2), (3,5-dibromo-4-hydroxyphenyl)(2-ethyl-6-methoxybenzofuran-3-yl)methanone (3), (5-bromo-2-ethyl-6-methoxybenzofuran-3-yl)(3,5-dibromo-4-hydroxyphenyl)methanone (4), (3,5-dibromo-4-hydroxyphenyl)(2-ethyl-6-hydroxybenzofuran-3-yl)methanone (5), (3,5-dibromo-4-hydroxyphenyl)(2-ethyl-5-methoxybenzofuran-3-yl)methanone (6), (4,6-dibromo-2-ethyl-5-hydroxybenzofuran-3-yl)(4-methoxyphenyl)methanone (7), (3,5-dibromo-4-hydroxyphenyl)(2-ethyl-5-hydroxybenzofuran-3-yl)methanone (8), (3,5-dibromo-4-hydroxyphenyl)(2-ethyl-5-fluorobenzofuran-3-yl)methanone (9), (2-ethylbenzofuran-3-yl)(3-fluoro-4-

hydroxyphenyl)methanone (10), (3-chloro-4-hydroxyphenyl)(2-ethylbenzofuran-3-yl)methanone (11), (3-bromo-4-hydroxyphenyl)(2-ethylbenzofuran-3-yl)methanone (12), (2-ethyl-5-methoxybenzofuran-7-yl)(4-methoxyphenyl)methanone (20), (3,5-dibromo-4-hydroxyphenyl)(2-ethyl-5-methoxybenzofuran-7-yl)methanone (21), (3,5-dibromo-4-hydroxyphenyl)(2-ethyl-5-hydroxybenzofuran-7-yl)methanone (22), (6-bromo-2-ethyl-7-hydroxybenzofuran-4-yl)(4-methoxyphenyl)methanone (23), (3,5-dibromo-4-hydroxyphenyl)(2-ethyl-5-methoxybenzofuran-4-yl)methanone (24), (3,5-dibromo-4-hydroxyphenyl)(2-ethyl-5-hydroxybenzofuran-4-yl)methanone (25), (6-bromo-2-ethyl-7-hydroxybenzofuran-4-yl)(3,5-dibromo-4-hydroxyphenyl)methanone (26).[10,11]

3-iodo-4-methoxybenzoyl chloride (27)

3-Iodo-4-methoxybenzoic acid (1.00 g, 7.19 mmol) was dissolved in $SOCl_2$ (12.0 mL) and stirred at 80°C (22 hours). Next, $SOCl_2$ was removed in vacuo and azeotroped twice with benzene to give (27) (700 mg, 2.36 mmol, 32%) as a white solid. ^{1}H-NMR (400 MHz) $CDCl_3$: 8.50 (s, 1 H), 8.12–8.10 (d, 1 H), 6.88–6.86 (d, 1 H), 3.99 (s, 3 H); ^{13}C-NMR (100 MHz) $CDCl_3$: 165.1, 162.8, 141.9, 133.2, 126.3, 109.4, 85.2, 56.2.

3,5-dichloro-4-hydroxybenzoyl chloride (28)

3,5-Dichloro-4-hydroxybenzoic acid (800 mg, 3.86 mmol) was dissolved in $SOCl_2$ (10.0 mL) and the reaction mixture stirred at room temperature (RT; 16 hours) and then heated to reflux (21 hours). Next, $SOCl_2$ was removed in vacuo and azeotroped twice with toluene to give (28) (540 mg, 2.40 mmol, 62%) as a brown solid. ^{1}H-NMR (400 MHz) $CDCl_3$: 8.07 (s, 2 H), 6.59 (bs, 1H); ^{13}C-NMR (100 MHz) $CDCl_3$: 165.5, 153.7, 131.5 126.4, 121.8.

4-methoxy-3,5-dimethylbenzoyl chloride (29)

3,5-Dimethyl-4-methoxy-benzoic acid (500 mg, 2.77 mmol) was dissolved in $SOCl_2$ (10.0 mL) and then stirred at RT (16 hours) and then heated to reflux (15 hours). Next, $SOCl_2$ was removed in vacuo and azeotroped twice with benzene to give (29) (530 mg, 2.67 mmol, 96%) as a white solid. ^{1}H-NMR (400 MHz) $CDCl_3$: 7.80 (s, 2 H), 3.79 (s, 3 H), 2.34 (s, 6 H).

3,5-di-tert-butyl-4-hydroxybenzoyl chloride (30)

3,5-Di-tert-butyl-4-hydroxybenzoic acid (500 mg, 2.00 mmol) was dissolved in $SOCl_2$ (7.0 mL) and heated to reflux (18 hours). Next, the contents were stirred at RT (16 hours) and then heated to 80°C for 4 hours. The $SOCl_2$ was then removed in vacuo and azeotroped twice with toluene to give (30) (500 mg, 1.86 mmol, 93%) as a white solid. ^{1}H-NMR (400 MHz) $CDCl_3$: 7.99 (s, 2 H), 5.97 (s, 1 H), 1.47 (s, 18 H).

(2-ethylbenzofuran-3-yl)(3-iodo-4-methoxyphenyl)methanone (31)

2-Ethylbenzofuran (200 mg, 1.37 mmol) was weighed into a dry round-bottomed flask (RBF; 25 mL) containing a stir bar (SB). The material was diluted in CS_2 (4.0 mL), capped, and an N_2 balloon attached. The contents were stirred and cooled in an ice bath (30 minutes). Next, (27) (475 mg, 1.78 mmol) was added followed by dropwise addition of tin (IV) chloride (0.22 mL). The contents were stirred (3 hours) at 0°C and slowly warmed to RT and stirred (16 hours). The reaction mixture was diluted with H_2O and extracted with EtOAc (4 × 20 mL). The combined organic layer was washed with HCl (0.5 N), H_2O, saturated $NaHCO_3$, and brine. The organic layer was dried (Na_2SO_4), filtered, and concentrated in vacuo. The crude material was purified by column chromatography on SiO_2 (100% Hex to 5% EtOAc in Hex) to give (31) (310 mg, 0.763 mmol, 56%) as a white solid. ^{1}H-NMR (400 MHz) $CDCl_3$: 8.32 (s, 1 H), 7.86–7.84 (d, 1 H), 7.50–7.48 (d, 1 H), 7.43–7.41 (d, 1 H), 7.31–7.27 (m, 1 H), 7.23–7.20 (m, 1 H), 6.88–6.86 (d, 1 H), 3.98 (s, 3 H), 2.93–2.87 (q, 2 H), 1.37–1.33 (t, 3 H); ^{13}C-NMR (100 MHz) $CDCl_3$: 189.0, 165.8, 161.6, 153.6, 140.9, 133.5, 131.6, 126.9, 124.4, 123.5, 121.1, 115.8, 111.0, 110.0, 85.7, 56.6, 21.8, 12.3.

(2-ethylbenzofuran-3-yl)(4-hydroxy-3-iodophenyl)methanone (13)

In an RBF (35 mL) containing an SB, (31) (200 mg, 0.492 mmol) was diluted with DMF (8.0 mL) and NaSEt (207 mg, 2.46 mmol) was added. The reaction mixture was heated to 110°C and stirred (16 hours). The reaction was quenched by the addition of saturated NH_4Cl and then extracted with EtOAc (4 × 20 mL). The combined organic layers were washed with brine, dried (Na_2SO_4), filtered, and concentrated in vacuo. The crude material was purified twice by column chromatography on SiO_2 (Hex:EtOAc; 4:1) to give (13) (40.0 mg, 0.102 mmol, 2%) as a white solid. ^{1}H-NMR (400 MHz) $CDCl_3$: 8.23 (s, 1 H), 7.78–7.75 (d, 1 H), 7.50–7.48 (d, 1 H), 7.42–7.40 (d, 1 H), 7.31–7.27 (m, 1 H), 7.23–7.20 (m, 1 H), 7.06–7.04 (d, 1 H), 6.17 (brs, 1 H), 2.94–2.88 (q, 2 H), 1.37–1.33 (t, 3 H); ^{13}C-NMR (100 MHz) $CDCl_3$: 189.1, 166.0, 158.8, 153.6, 140.2, 133.6, 132.0, 126.8, 124.4, 123.6, 121.1, 115.7, 111.0, 85.5, 21.9, 12.3. LC/MS-MS: 393.0 → 246.9 m/z; GS1 and GS2 at 30, DP = 86, CE = 35, CXP = 16, t_R = 4.56 minutes.

(3,5-di-tert-butyl-4-hydroxyphenyl) (2-ethylbenzofuran-3-yl)methanone (14)

2-Ethylbenzofuran (200 mg, 1.37 mmol) was weighed out into a dry RBF (25 mL) containing an SB. The material was diluted in CS_2 (4.0 mL), capped, and an N_2 balloon attached. The contents were stirred and cooled in an ice bath (30 minutes). Next, (30) (478 mg, 1.78 mmol) was added followed by the dropwise addition of tin (IV) chloride (0.22 mL; 1.78 mmol). The contents were stirred (3 hours) at 0°C and slowly warmed to RT and stirred (16 hours). The reaction mixture was diluted with H_2O and extracted with EtOAc (4 × 20 mL). The combined organic layer was washed with HCl (0.5 N), H_2O, saturated $NaHCO_3$, and brine. The organic layer was dried (Na_2SO_4), filtered, and concentrated in vacuo. The crude material was purified by column chromatography on SiO_2 (90% Hex and 10% EtOAc) to give (14) (250 mg, 0.660 mmol, 48%) as a yellow oil. ^{1}H-NMR (400 MHz) $CDCl_3$: 7.77 (s, 2 H), 7.49–7.43 (dd, 2 H), 7.29–7.26 (m, 1 H), 7.21–7.17 (t, 1 H), 5.74 (s, 1 H), 2.96–2.91 (q, 2 H), 1.43 (s, 18 H), 1.37–1.33 (t, 3 H); ^{13}C-NMR (100 MHz) $CDCl_3$: 191.1, 165.4, 158.4, 153.6, 135.7, 130.4, 127.4, 127.2, 124.1, 123.1, 121.5, 116.3, 110.9, 34.4, 30.2, 21.8, 12.4. LC/MS-MS: 379.2 → 1731 m/z; GS1 and GS2 at 30, DP = 46, CE = 39, CXP = 10, t_R = 5.65 minutes.

(2-ethylbenzofuran-3-yl)(4-methoxy-3,5-dimethylphenyl)methanone (32)

2-Ethylbenzofuran (300 mg, 2.05 mmol) was weighed into a dry RBF (25 mL) containing an SB. The material was diluted in CS_2 (6.0 mL), capped, and an N_2 balloon attached. The contents were stirred and cooled in an ice bath (30 minutes). Next, (29) (530 mg, 2.67 mmol) was slowly added followed by dropwise addition of tin (IV) chloride (0.33 mL; 2.67 mmol). The contents were stirred (3 hours) at 0°C and then slowly warmed to RT and stirred (16 hours). The reaction mixture was diluted with H_2O and extracted with EtOAc (4 × 20 mL). The combined organic layer was washed with HCl (0.5 N), H_2O, saturated $NaHCO_3$, and brine. The organic layer was dried (Na_2SO_4), filtered, and concentrated in vacuo. The crude material was purified by column chromatography on SiO_2 (100% Hex to 5% EtOAc in Hex) to give (32) (248 mg, 0.804 mmol, 39%) as a clear oil. ^{1}H-NMR (400 MHz) $CDCl_3$: 7.53 (s, 2 H), 7.49–7.45 (t, 2 H), 7.30–7.26 (m, 1 H), 7.22–7.19 (t, 1 H), 3.80 (s, 3 H), 2.91–2.85 (q, 2 H), 2.32 (s, 6 H), 1.35–1.31 (t, 3 H); ^{13}C-NMR (100 MHz) $CDCl_3$: 191.3, 165.6, 161.0, 153.6, 134.8, 131.1, 130.2, 127.2, 124.2, 123.4, 121.3, 116.2, 110.9, 59.7, 21.8, 16.1, 12.3.

(2-ethylbenzofuran-3-yl)(4-hydroxy-3,5-dimethylphenyl)methanone (15)

In an RBF (35 mL) containing an SB, (32) (200 mg, 0.649 mmol) was diluted with DMF (10.0 mL) and NaSEt (218 mg, 2.59 mmol) was added. The reaction mixture was heated to 110°C and stirred (16 hours). The reaction was quenched by the addition of saturated NH_4Cl and extracted with EtOAc. The combined organic layers were washed with brine, dried (Na_2SO_4), filtered, and concentrated in vacuo. The crude material was purified by column chromatography on SiO_2 (Hex:EtOAc; 4:1) to give (15) (30.0 mg, 0.102 mmol, 16%) as a light yellow oil. ^{1}H-NMR (400 MHz) $CDCl_3$: 7.55 (s, 2 H), 7.49–7.46 (m, 2 H), 7.30–7.26 (m, 1 H), 7.22–7.18 (t, 1 H), 5.77 (s, 1 H), 2.91–2.86 (q, 2 H), 2.26 (s, 6 H), 1.35–1.32 (t, 3 H); ^{13}C-NMR (100 MHz) $CDCl_3$: 191.2, 165.1, 157.0, 153.6, 131.2, 130.6, 127.3, 124.2, 123.3, 123.2, 121.3, 116.3, 110.9, 21.8, 15.9, 12.3. LC/MS-MS: 294.8 → 173.2 m/z; GS1 and GS2 at 30, DP = 16, CE = 29, CXP = 18, t_R = 4.49 minutes.

(3,5-dibromo-4-methoxyphenyl)(2-ethylbenzofuran-3-yl)methanone (16)

In an RBF (25 mL) containing an SB, (1) (100 mg, 0.236 mmol) was diluted with THF (2.0 mL) and K_2CO_3 (37.0 mg, 0.259 mmol) was added. The reaction mixture was stirred (10 minutes) and iodo-methane (16.0 µL, 0.259 mmol) was added and stirred at 40°C (16 hours). The reaction was diluted with H_2O and extracted with EtOAc (3 × 10 mL). The combined organic layers were washed with brine, dried (Na_2SO_4), filtered, and concentrated in vacuo. The crude material was purified by column chromatography on SiO_2 (Hex:EtOAc; 6:1) to give (16) (22.0 mg, 0.050 mmol, 22%). ^{1}H-NMR (400 MHz) $CDCl_3$: 7.99 (s, 2 H), 7.51–7.49 (d, 1 H), 7.43–7.41 (d, 1 H), 7.33–7.30 (t, 1 H), 7.26–7.25 (m, 1 H), 3.98 (s, 3 H), 2.93–2.88 (q, 2 H), 1.38–1.34 (t, 3 H); ^{13}C-NMR (100 MHz) $CDCl_3$: 188.0, 166.9, 157.7, 153.7, 137.2, 133.6, 126.4, 124.7, 123.9, 121.0, 118.5, 115.3, 111.1, 60.8, 22.0, 12.2. LC/MS-MS: 439.0 → 292.7 m/z; GS1 and GS2 at 30, DP = 91, CE = 35, CXP = 18, t_R = 5.68 minutes.

(2-butylbenzofuran-3-yl)(4-methoxyphenyl) methanone (33)

2-Butylbenzofuran (400 mg, 2.30 mmol) was weighed out into a dry RBF (25 mL) containing an SB. The material was diluted in CS_2 (6.0 mL), capped, and an N_2 balloon attached. The mixture was stirred and cooled in an ice bath (30 minutes). Next, 4-methoxybenzoyl chloride (404 µL, 2.98 mmol) was added followed by dropwise addition of

tin (IV) chloride (370 µL, 2.98 mmol). The contents were stirred (3 hours) at 0°C and slowly warmed to RT and stirred (3 days). The reaction mixture was diluted with H_2O and extracted with EtOAc (4 × 12 mL). The combined organic layer was washed with HCl (0.5 N), H_2O, saturated $NaHCO_3$, and brine. The organic layer was dried (Na_2SO_4), filtered, and concentrated in vacuo. The crude material was purified by column chromatography on SiO_2 (100% Hex to 5% EtOAc in Hex) to give (33) (455 mg, 1.48 mmol, 64%) as a clear oil. ^{1}H-NMR (400 MHz) $CDCl_3$: 7.87–7.85 (d, 2 H), 7.49–7.47 (d, 1 H), 7.38–7.36 (d, 1 H), 7.28–7.25 (m, 1 H), 7.20–7.16 (m, 1 H), 6.97–6.95 (d, 2 H), 3.88 (s, 3 H), 2.95–2.91 (t, 2 H) 1.79–1.75 (m, 2 H), 1.40–1.34 (m, 2 H), 0.92–0.88 (t, 3 H); ^{13}C-NMR (100 MHz) $CDCl_3$: 190.5, 164.6, 163.4, 153.6, 131.9, 131.7, 127.2, 124.1, 123.3, 121.2, 116.8, 113.7, 111.9, 55.5, 30.2, 27.8, 22.4, 13.7.

(2-butylbenzofuran-3-yl)(4-hydroxyphenyl) methanone (17)

In an RBF (100 mL) containing an SB, (33) (400 mg, 1.30 mmol) was diluted with DMF (18.0 mL) and NaSEt (426 mg, 5.19 mmol) was added. The reaction mixture was heated to 110°C and stirred (16 hours). The reaction was quenched by the addition of saturated NH_4Cl and was extracted with EtOAc (4 × 25 mL). The combined organic layers were washed with brine, dried (Na_2SO_4), filtered, and concentrated in vacuo. The crude material was purified by column chromatography on SiO_2 (Hex:EtOAc; 4:1) to afford (17) (210 mg, 0.713 mmol, 55%) as a light yellow oil. ^{1}H-NMR (400 MHz) $CDCl_3$: 7.81–7.78 (d, 2 H), 7.48–7.46 (d, 1 H), 7.37–7.36 (d, 1 H), 7.29–7.25 (m, 1 H), 7.20–7.16 (m, 1 H), 6.94–6.90 (d, 2 H), 6.56 (bs, 1 H), 2.93–2.89 (t, 2 H) 1.79–1.71 (m, 2 H), 1.38–1.32 (m, 2 H), 0.90–0.86 (t, 3 H); ^{13}C-NMR (100 MHz) $CDCl_3$: 191.2, 165.0, 160.4, 153.6, 132.1, 131.6, 127.1, 124.2, 123.4, 121.2, 116.7, 115.4, 111.0, 30.1, 27.9, 22.3, 13.7. LC/MS-MS: 295.0 → 121.2 m/z; GS1 and GS2 at 30, DP = 56, CE = 31, CXP = 6, t_R = 4.51 minutes.

(2-butylbenzofuran-3-yl)(3,5-dibromo-4-hydroxyphenyl)methanone (18)

In an RBF (15 mL) containing an SB, NBS (48.0 mg, 0.272 mmol) in DCM (2.0 mL) was treated with DMF (40 µL) at −10°C (ice-brine cooling bath) for 10 minutes. Then, a solution of (17) (40.0 mg, 0.136 mmol) in DCM (2.0 mL) was added. The reaction mixture was slowly warmed to RT and stirred (17 hours). The reaction was quenched with H_2O, additional DCM added, and the organic layer washed with water (4 × 8 mL) and brine. The organic layer was dried (Na_2SO_4), filtered, and concentrated under reduced pressure. The crude material was purified twice by column chromatography on SiO_2 (Hex:EtOAc; 4:1) to afford (18) (27.0 mg, 0.060 mmol, 44%) as a light yellow oil. ^{1}H-NMR (400 MHz) $CDCl_3$: 7.98 (s, 2 H), 7.50–7.48 (d, 1 H), 7.40–7.38 (d, 1 H), 7.32–7.29 (m, 1 H), 7.26–7.21 (m, 1 H), 6.36 (bs, 1 H), 2.91–2.87 (t, 2 H) 1.82–1.74 (m, 2 H), 1.42–1.33 (m, 2 H), 0.94–0.88 (t, 3 H); ^{13}C-NMR (100 MHz) $CDCl_3$: 187.0, 165.0, 152.9, 152.3, 132.9, 132.7, 125.8, 123.8, 123.0, 120.2, 115.1, 110.4, 109.2, 29.3, 27.3, 21.7, 12.9. LC/MS-MS: 452.9 → 278.9 m/z; GS1 and GS2 at 30, DP = 101, CE = 37, CXP = 16, t_R = 7.82 minutes.

(3,5-dichloro-4-hydroxyphenyl)(2-ethylbenzofuran-3-yl)methanone (19)

2-Ethylbenzofuran, (200 mg, 1.37 mmol) was weighed out into a dry RBF (25 mL) containing an SB. The material was diluted in CS_2 (4.0 mL), capped, and an N_2 balloon attached. The contents were stirred and cooled in an ice bath (30 minutes). Next, (28) (401 mg, 1.78 mmol) was added followed by dropwise addition of tin (IV) chloride (0.22 mL). The contents were stirred (3 hours) at 0°C and slowly warmed to RT and stirred (16 hours). The reaction mixture was diluted with H_2O and extracted with EtOAc (4 × 20 mL). The combined organic layer was washed with HCl (0.5 N), H_2O, saturated $NaHCO_3$, and brine. The organic layer was dried (Na_2SO_4), filtered, and concentrated in vacuo. The crude material was purified three times by column chromatography on SiO_2 (100% Hex to 5% EtOAc in Hex) to give (19) (30.0 mg, 0.089 mmol, 7%) as an off-white solid. ^{1}H-NMR (400 MHz) $CDCl_3$: 8.31 (s,1 H), 7.88 (s, 2H), 7.53–7.51 (d, 1 H), 7.42–7.40 (d, 1 H), 7.35–7.31 (m, 1 H), 2.98–2.92 (q, 2 H), 1.40–1.36 (t, 3 H); ^{13}C-NMR (100 MHz) $CDCl_3$: 190.1, 168.1, 155.9, 152.4, 130.9, 129.1, 125.8, 124.5, 123.6, 123.5, 120.5, 120.4, 111.3, 21.7, 12.9. LC/MS-MS: 339.1 → 146.2 m/z; GS1 and GS2 at 30, DP = 71, CE = 35, CXP = 8, t_R = 4.64 minutes.

(2-ethylbenzofuran-3-yl)(2,3,4,5,6-pentadeuteriophenyl)methanone (34)

2-Ethylbenzofuran (386 mg, 2.64 mmol) was weighed out into a dry RBF (25 mL) containing an SB. The material was diluted in CS_2 (8.0 mL), capped, and an N_2 balloon was attached. The contents were stirred and cooled in an ice bath (30 minutes). Benzoyl chloride-d_5 (399 µL, 3.43 mmol) was added slowly; next, tin (IV) chloride (0.40 mL) was added drop-wise. The contents were stirred (3.0 hours) at 0°C and

then allowed to slowly warm to RT and stirred (3 days). The reaction mixture was diluted with H_2O and extracted with EtOAc (4 × 20 mL). The combined organic layer was washed with HCl (0.5 N, 3.0 mL), water, saturated $NaHCO_3$, and brine. The organic layer was dried (Na_2SO_4), filtered, and concentrated in vacuo. The compound was purified twice by column chromatography on SiO_2 (Hex:EtOAc; 4:1) to give (34) (270 mg, 1.06 mmol, 40%) as a yellow oil, which solidified upon sitting. ^{1}H-NMR (400 MHz) $CDCl_3$: 7.50–7.48 (d, 1 H), 7.39–7.37 (d, 1 H), 7.29–7.26 (m, 1 H), 7.21–7.17 (m, 1 H), 2.94–2.88 (q, 2 H), 1.36–1.32 (t, 3 H); ^{13}C-NMR (100 MHz) $CDCl_3$: 192.0, 166.5, 153.7, 139.3, 132.2 (t, CD), 128.7 (t, 2CD), 128.0 (t, 2CD), 127.0, 124.4, 123.5, 121.4, 116.1, 111.0, 21.9, 12.3. LC/MS-MS: 256.2 → 109.9 m/z; GS1 and GS2 at 30, DP = 36, CE = 27, CXP = 6, t_R = 4.78 minutes.

Incubations

Test compounds were freshly prepared as stock solutions in DMSO (20.0 mM). Immediately prior to experiments, aqueous drug solutions (10.0 µM) were prepared. To probe in vitro metabolism, rat liver, and rat intestine incubations were conducted at 37.0°C ± 0.1°C and included (final concentration) 0.20 mg/mL microsomal protein with various cofactors and/or reagents such as NADPH (1.0 mM, cofactor for mono-oxygenases, eg, cytochrome P450), UDPGA (4.0 mM, cofactor for glucuronidation; eg, UGTs), alamethicin (42 µg/mg protein), and 1.0 µM test compound (DMSO ≤ 0.002%, total v/v). Incubations consisted of phosphate buffer (100 mM; pH 7.4), $MgCl_2$ (5.0 mM), and EDTA (0.1 mM). Incubations were performed as follows: (1) a mixture of phosphate buffer, $MgCl_2$, UDPGA and/or NADPH, alamethicin, and microsomal protein were preincubated at 37.0°C ± 0.1°C for 10 minutes; and (2) incubations were initiated by test compound addition and mixing (1.0 µM final), also preincubated at 37.0°C ± 0.1°C. After initiation (0.5 minutes) and at 5, 10, 15, 30, and 60 minutes, incubate samples were removed and added to three volumes of quench solution (cold acetonitrile). The resulting samples were mixed and immediately analyzed by LC/MS-MS.

Rat pharmacokinetic studies

The in vivo portion was conducted at East Tennessee State University, Quillen College of Medicine (Johnson City, TN), in an Association for Assessment and Accreditation of Laboratory Animal Care International accredited facility. All procedures were reviewed and approved by the East Tennessee State University Committee on Animal Care; the research procedures adhered to the Principles of Laboratory Animal Care (National Institutes of Health publication No 85-23, revised in 1985). Male Sprague-Dawley rats were purchased from Harlan World Headquarters (Indianapolis, IN). Animals were housed in groups of three at 22.2°C ± 1.1°C and 55% ± 15% humidity with 12-hour dark–light cycles. Dosing was conducted 2.0–3.0 hours after the beginning of a light cycle. All animals had free access to water but fasted 12–15 hours prior to dosing in cages with bedding; food was returned 4 hours postdose. Fasted animals (264 ± 13 g) were dosed either (1) via the ophthalmic venous plexus (orbital sinus) using a 1.0 mL disposable syringe with a 27G needle; or (2) via capsule dosing using a Torpac capsule syringe (Torpac, Fairfield, NJ) immediately followed with a bolus of HPLC grade H_2O (500 µL). CMC formulations were prepared by weighing synthesized compound into a glass vial and adding four weight equivalents of CMC. A stir vane was added, capped, and stirred (1.0 hour). Thereafter, to help remove clumps or aggregates that might have formed while mixing, the materials were removed and passed through a 35-mesh sieve screen. After additional mixing, the blend containing approximately 20 weight percent was used to prepare capsules. The 6-methoxy-benzbromarone (3)/HBenβCD (hydroxybutenyl-beta-cyclodextrin) was prepared using methods analogous to those previously described.[12,13] Briefly, an aqueous ethanol suspension of (3) was mixed with four weight equivalents of HBenβCD, warmed, and vortex-mixed to afford a solution. EtOH was removed under reduced pressure, and additional water was added, frozen with liquid nitrogen, and lyophilized (30 hours) to a dry solid. The formulation was mixed and passed through a 35-mesh sieve screen and subsequently used to prepare capsules. Using a filling funnel, formulations were encapsulated into hard shell Torpac Lock ring gel (size 9) capsules (Torpac). Ophthalmic venous plexus doses were prepared immediately prior to dosing as aqueous solutions containing 10% DMSO; these rats were anesthetized with isoflurane and subsequently infused (300 µL over <30 seconds) with corresponding drug solution via the ophthalmic venous plexus (orbital sinus). Using tail-vein collection (the anterior portion was transected 2–3 mm), blood samples (125 µL) were collected using mini-capillary blood collection tubes containing EDTA di-potassium salt (SAFE-T-FILL®; RAM Scientific Inc, Yonkers, NY). Animals administered compounds orally had blood samples taken at 0.5, 1.0, 2.0, 3.0, 4.0, 6.0, 8.0, 24.0, and 48.0 hours postdose, whereas intravenous administration (orbital sinus) time points were 0.083, 0.33, 0.67, 1.0, 2.0, 4.0, 6.0, 8.0, and 10.0 hours postdose. Immediately after filling, individual sample tubes were mixed and stored on dry ice and kept frozen (–80°C ± 10°C)

until sample preparation and subsequent LC/MS-MS analysis. Control rat blood collected with K_2 EDTA (Lot No 163458) was purchased from Bioreclamation LLC (Westbury, NY). The control blood was used to prepare individual compound standard curves, which were used to compute apparent in vivo blood concentration data. Standard curves (SC) were prepared by addition with thorough mixing of various aqueous solutions (50 µL) into control blood (950 µL). SC samples were mixed and immediately frozen (–80°C ± 10°C). SC samples were extracted and processed in an analogous fashion as in vivo samples as follows: an extraction solution containing deuterated 34 (0.2 µM) as the internal standard (IS) was freshly prepared in a 100 mL volumetric flask containing 4:1 ACN:MeOH (1:1) and H_2O (v/v) in individual sets. The PK sample tubes were removed from the freezer (–80°C ± 10°C) and allowed to thaw on ice (20–30 minutes). The tubes were vortex-mixed (3–5 seconds) followed by extraction solution (250 µL) addition, vortex-mixed (5 seconds) again, saturated at RT for 5.0 minutes, vortex-mixed an additional time (5 seconds), and centrifuged at 10,000 rpm (10 minutes) using an Eppendorf minispin centrifuge (Hamburg, Germany). The supernatants were transferred into individual wells of a 96-well plate. The 96-well plate was placed into the LEAP auto-sampler cool-stack (6.0°C ± 0.1°C) and immediately analyzed via LC/MS-MS.

Data analysis and statistical methods

The in vitro microsomal data were analyzed and expressed as percentage disappearance of parent compound relative to the 30 second time sample. The in vitro $T_{1/2}$ values were obtained from the slope of the nonlinear regression via the percentage remaining versus incubation time relationship (–k) as follows: in vitro $T_{1/2} = -0.693/k$. The results were used to calculate in vitro intrinsic clearance (CL_{int}, µL/min/mg protein) similar to previously described methods.[14] PK data were computed using noncompartmental analysis model via linear trapezoidal rule via software program WinNonlin® (v5.3; Pharsight, St Louis, MO). Analyst 1.4.2 (Applied Biosystems, Framingham, MA) was used for LC/MS-MS data acquisition. Prism 4.02™ (GraphPad Software, Inc; San Diego, CA) was used to graph and perform statistical analysis. The statistical differences between compounds 10–13 were compared using one-way analysis of variance followed by a Tukey–Kramer comparison test at the 95% confidence level. The statistical differences between individual compounds incubated with rat liver microsomes with and without UDPGA were compared using an unpaired *t*-test with Welch's correction. The statistical differences between specifically discussed IC_{50} value comparisons and F_a comparisons were also compared using an unpaired *t*-test with Welch's correction with an F test to compare variances. Chemical structures were prepared using ChemBioDraw Ultra 12.0 (CambridgeSoft; Cambridge, MA), and the tPSA (polar surface area) and CLogP values were obtained via the chemical properties feature.

Results

Inhibitor structure–activity relationship

As we had unanswered questions regarding the hURAT1 inhibitor SAR, we prepared additional compounds ([13]–[19]; Table 1). Using the previously described in vitro screening method, we tested the additional compounds for their ability to inhibit ^{14}C-urate uptake in oocytes expressing hURAT1 (SLC22A12).[10] Mono-iodo (13) was prepared to complete the mono-halogen comparison (ie, F, Cl, Br, and I). The data illustrate that electronic and steric effects influence inhibition potency; Cl ≈ Br > I > F (IC_{50} [11] ≈ [12] < [13] < [10]). Chloro analog (11) and bromo analog (12) were not statistically different, whereas all other comparisons were statistically significant ($P < 0.001$). To further probe electronic versus steric effects, we prepared tert-butyl analog (14) and di-methyl (15). Di-methyl (15) had an in vitro IC_{50} of approximately 7.5 µM, whereas (14) was a much weaker inhibitor (>25 µM). We also synthesized methoxy ether (16), a molecule that does not produce the corresponding anion; thus, (16) is a C-ring methoxy analog of benzbromarone 1.[11] Compound 16 was a much weaker inhibitor, ~47-fold (1.2 µM versus 26 nM). We also prepared butyl analogs (17) and (18). Nonhalogenated butyl analog (17) was a much weaker inhibitor than the corresponding ethyl analog.[10] Compound (18) (1932 nM) compared with (1) (26 nM) also clearly demonstrates the alkyl chain modification effect. Lastly, as mono-chloro 11 (874 nM) and mono-bromo 12 (814 nM) were not statistically different in the in vitro assay, we prepared di-chloro 19 (379 nM), which exhibited weaker inhibitor (~15-fold) than (1) (26 nM).

Rat liver incubations

Representative compounds from all three templates were investigated and the data summarized in Table 2. Rat liver microsomal incubations were conducted in the presence of UDPGA and/or NADPH. The NADPH data demonstrate the extent to which the corresponding compound was metabolized via Phase I oxidation, whereas NADPH/UDPGA represents both oxidation and/or Phase II glucuronidation pathways. Higher intrinsic clearance (CL_{int}) values equate to a faster

Table 2 Rat liver microsomal intrinsic clearance (CL_{int}; µL incubation/mg protein; n = 3 ± SD)

Compound	NADPH	NADPH and UDPGA
Verapamil	241.4 ± 6.7	248.4 ± 0.8 ns
(1)	43.0 ± 2.3	51.3 ± 6.7 ns
(2)	61.6 ± 2.6	412.1 ± 6.4***
(3)	117.7 ± 8.7	207.3 ± 4.2**
(4)	24.8 ± 1.9	23.5 ± 10.9 ns
(5)	23.0 ± 2.9	19.7 ± 2.8 ns
(6)	9.5 ± 2.8	44.9 ± 6.6*
(7)	269.3 ± 2.5	286.8 ± 0.9**
(8)	43.7 ± 2.9	52.0 ± 0.1*
(9)	142.8 ± 1.7	142.1 ± 5.5 ns
(20)	548.9 ± 11.5	703.5 ± 12.7***
(21)	8.5 ± 2.0	209.5 ± 5.9***
(22)	11.2 ± 3.3	454.5 ± 18.2***
(23)	42.8 ± 1.4	121.0 ± 12.2**
(24)	6.2 ± 0.6	323.2 ± 10.8***
(25)	70.2 ± 1.7	94.8 ± 5.1*
(26)	2.6 ± 1.0	34.3 ± 1.2***

Notes: *$P < 0.05$; **$P < 0.01$; ***$P < 0.001$.
Abbreviations: NADPH, nicotinamide adenine dinucleotide phosphate; ns, not significant; SD, standard deviation; UDPGA, UDP-glucuronic acid.

in vitro metabolism rate. For each compound, the NADPH results versus NADPH/UDPGA were compared statistically. Compounds (1), (4), (5), and (9) displayed no statistical difference in the presence of the Phase II cofactor UDPGA.

Bioanalytical pharmacokinetic summary

For each compound investigated, eight-point standard curves (n = 4 ± standard deviation [SD]) representing concentrations between 1 ng/mL and 5600 ng/mL were prepared. All standard curve data were fitted to a $1/x^2$ weighted linear regression; compounds 1, 3, 5, 6, 8, and 9 displayed correlation coefficients (R^2) of 0.9942, 0.9953, 0.9948, 0.9967, 0.9980, and 0.9980, respectively. The limits of detection (LOD) from rat blood were ~2.2 ng/mL, whereas the limits of quantification (LOQ) from extracted rat blood ranged between 9 ng/mL and 12 ng/mL. Compiled in Table 3, the data for the in vivo PK studies performed in male Sprague-Dawley rats were computed via noncompartmental modeling; C_{max}, T_{max}, $T_{1/2}$, $AUC_{0-\infty}$, and F_a are listed.

Discussion

Inhibitor structure–activity relationship

We have prepared and tested additional (2-alkyl-benzofuran-3-yl)(3,4,5-substituted-phenyl)methanone compounds not previously described.[10,11] Three constitutional isomer templates (Figure 1) were probed; compounds (1)–(19), (20)–(22), and (23)–(26) are template I, II, and III examples, respectively. The data support the notion that hURAT1 has a positively charged binding pocket and that important Coulombic interactions on the C-ring (Figure 1) are required for substrate (uric acid; pKa 5.4 in urine) and inhibitor recognition. We previously illustrated that phenols (C-ring; R_3 = –OH) display a linear relationship regarding pKa and their computed phenol anion charge.[11] Analogs with higher pKa values are weaker hURAT1 substrates and inhibitors. For example, 2-halophenols (F, Cl, Br, and I) and 2,6-dihalophenols (di-Cl and di-Br) have pKa values of 8.8, 8.5, 8.4, 8.5, 6.8, and 6.7, respectively. The least acidic 2-fluorophenol has the weakest anion:hURAT1 affinity. Representing C-ring modification in template I (C-ring; R_3 = –OH; R_2 = –F, –Cl, –Br, –I; [10]–[13]; Table 1), both electronic and steric effects are important. Comparing the mono-halo series, mono-fluoro 10 has the highest pKa value and was observed to be the weakest inhibitor via the in vitro ^{14}C-urate uptake screen (Table 1; IC_{50} [11] ≈ [12] < [13] < [10]). Chloro (11) and bromo (12) inhibition data were not statistically different, but all other mono-halogen comparisons were statistically significant ($P < 0.001$). Although phenol pKa plays an important factor, steric interactions near the anion are clearly important too. Iodo (13) was a weaker inhibitor (higher IC_{50} value) than chloro (11) and bromo (12); hence, bulky groups ortho to the phenol distort the anion:hURAT1 interface and produce weaker inhibitors. To further probe steric effects versus halogen effects, we prepared and tested tert-butyl analog (14) and di-methyl (15). Alkyl groups are known to participate in a delocalization process called hyperconjugation.[15] As the two di-alkyl phenols 2,6-di-tert-butyl-phenol and 2,6-dimethyl-phenol have similar pKa values (10.2 and 10.7, respectively), their corresponding anion concentrations

Table 3 Orbital sinus rat pharmacokinetic summary (n = 3 ± SD)

Orbital sinus	Dose mg/kg	T_{max} hours	$T_{1/2}$ hours	AUC µg·h/mL
(1)	0.5		1.1 ± 0.1	9.07 ± 0.59
(M) (5)		0.9 ± 0.2	4.3 ± 0.1	0.92 ± 0.11
(3)	0.5		1.4 ± 0.6	9.60 ± 0.28
(M) (5)		2.7 ± 0.3	0.4 ± 0.2	4.26 ± 0.47
(5)	0.5		4.0 ± 1.4	6.16 ± 0.68
(6)	0.5		1.3 ± 0.1	2.63 ± 0.25
(M) (8)		0.7 ± 0.3	1.7 ± 0.2	0.70 ± 0.14
(8)	0.5		1.5 ± 0.5	0.94 ± 0.08
(9)	0.5		1.2 ± 0.1	5.26 ± 0.81

Abbreviations: AUC, area under the curve; M, active metabolite formed in vivo and monitored by liquid chromatography/mass spectrometry-mass spectrometry; SD, standard deviation; $T_{1/2}$, half-life; T_{max}, time after administration to achieve peak blood concentration.

under the in vitro test conditions are expected to be comparable.[11] Although slightly more acidic, the bulky di-tert-butyl analog (14) was a weaker inhibitor (>25 μM) than the di-methyl (15) analog (IC_{50} 7.5 μM). Therefore, C-ring phenols with bulky ortho-substituents (iodo or tert-butyl) are weaker hURAT1 inhibitors than their corresponding chloro and bromo analogs. As the experimental data supported the notion that a potent hURAT1 inhibitor requires an anion (a formal negative charge) to interact with the positively charged binding pocket, we attempted to delineate the importance of the anion within chemical template I. We prepared methoxy ether (16), a molecule that does not produce the corresponding anion. Compound (16) was a much weaker inhibitor, ~47-fold (1.2 μM versus 26 nM). These data further illustrate the importance of the required anion:hURAT1 interaction. In addition to the C-ring modifications, we also probed the 2-alkyl position (R_1) within the benzofuran. We prepared butyl analogs (17) and (18). Butyl analog (17) was a much weaker inhibitor than the corresponding ethyl analog.[10] Likewise, compound (18) produced a nice comparison with ethyl analog (1), displaying weaker inhibition (1.9 μM). Lastly, as mono-chloro (11) and mono-bromo (12) were not statistically different in the in vitro assay, we also prepared and tested di-chloro (19); (19) was a weaker inhibitor (~15-fold) than (1). All of these experimental data demonstrate that an ideal hURAT1 inhibitor pertaining to this chemical template should contain a phenol in the C-ring (R_3 = –OH). The most desirable compounds have pKa values lower than uric acid and are o,o-di-bromo analogs, which circumvent phenol-keto tautomerism.[11,15] In addition to the importance of the C-ring, substituent effects on the B-ring are also important to afford very potent inhibitors. Comparing the 6-position within the benzofuran (B-ring, R_5; –H, –OMe and –OH; (1), (3), and (5); IC_{50} 26, 111, and 138 nM, respectively), electronically donating groups (–OMe and –OH versus –H) produced weaker in vitro inhibitors. Comparing the 5-position within the benzofuran (B-ring, R_6; –H, –OMe, –OH, –F; (1), (6), (8), and (9); IC_{50} 26, 42, 189, and 6 nM, respectively), electronically donating groups (–OMe and –OH versus –H) result in weaker hURAT1 inhibitors, whereas the inductively withdrawing fluoro analog (9) produced a more potent inhibitor. At this stage, having established a relationship regarding structure and inhibitor potential, we sought to metabolically probe the most promising drug candidates generated from our SAR findings. We used an in vitro hepatic assay employing LC/MS-MS analysis to generate hepatic intrinsic clearance (CL_{int}) values.

In vitro metabolism

As summarized in Table 2, we conducted an in vitro screen to investigate in vitro hepatic metabolism for compounds (1)–(9) and (20)–(26); these compound examples represent all three templates (I, II, and III; Figure 1). Rat liver microsomal incubations were conducted in the presence of NADPH or NADPH/UDPGA; NADPH being the cofactor required for Phase I CYP P450 oxidations, whereas UDPGA is the cofactor required for Phase II glucuronidation. The observed intrinsic clearance (CL_{int}) values represent in vitro metabolism rates, with the larger values equate to faster in vitro metabolism. We commonly use a control drug (verapamil) to confirm viable microsomes.[16] The NADPH versus NADPH/UDPGA comparisons provide biotransformation trends; Table 2 includes the statistical comparison for each compound tested. Using these screening data, compounds (1), (4), (5), and (9) did not display a statistical difference in metabolism rate when UDPGA was also present. Other compounds displayed statistical differences; for example, compounds (6), (8), and (25) were slightly different ($P < 0.05$), whereas (3), (7), and (23) were moderately different ($P < 0.01$), and (2), (20)–(22), (24), and (26) were very significant ($P < 0.001$). These in vitro results provide general conclusions. Moderately bulky ortho-ortho-dihalo-phenol functionality (C-ring) appears to protect the phenol from undergoing Phase II glucuronidation (compare [2] versus [6]). B-ring analogs with methoxy functionality ([3] and [6]; Table 2 and Figure 2) experience tandem in vitro Phase I/Phase II biotransformation. B-ring oxidative de-methylation of (3) and (6) produced phenol (5) and (8), respectively; however, compared with incubations of phenol (5) and (8), methoxy analogs (3) and (6) produced higher levels of Phase II glucuronides (35) and (36), respectively (see Supplementary materials). The location of the methoxy functionality on the B-ring clearly plays an electronic and/or steric effect, influencing both metabolism rate and inhibitor potency (Table 1). Comparing (3) versus (6) (Table 2), 6-methoxy (3) was metabolized at a faster rate than 5-methoxy (6). All tested analogs comprising template II having the C-ring connectivity occurring at the 7-position in the benzofuran, compounds (20)–(22), produced significant Phase II in vitro glucuronidation. Template III compounds with connectivity occurring at benzofuran position-4 displayed similar trends as previously described for template I.

In vivo metabolism and pharmacokinetics

We had two major factors influencing our decision regarding which compounds to move forward and investigate in vivo: (1) the molecule should have a good (low) IC_{50}

value in the in vitro oocyte screen (Table 1); hence, the following were potential candidates: (1), (3), (5), (6), (8), (9), (19), (22), (25), and (26); and (2) the relative accessibility of analogs via our chemical synthesis methods, a factor which excluded compound (19) and template II and III compounds (22), (25), and (26). We selected and tested six template I compounds ([1], [3], [5], [6], [8], and [9]). The intravenous dosing experiments were conducted using drug solutions and orbital sinus administration. For all in vivo experiments, blood samples were collected via tail vein, mixed, and immediately frozen. After thawing, samples were mixed and extracted with an aqueous organic solvent containing an internal standard. The centrifuged supernatants were analyzed using LC/MS-MS methods. The intravenous (orbital sinus) dose (0.5 mg/kg) data are summarized in Table 3. Consistent with in vitro metabolism observations, in vivo Phase I oxidation of benzbromarone (1) (Figure 2; Table 2) afforded 6-hydroxy-benzbromarone (5) as the major metabolite; metabolite (5) is a potent hURAT1 inhibitor (Table 1). The $T_{1/2}$ of (1) was fast (1 hour), whereas the metabolite (5) displayed a longer $T_{1/2}$ (4 hours) with a T_{max} 1 hour postdose (Table 3). Compared with the parent drug, the amounts of (5) formed from biotransformation of (1) orally (16.4 mg/kg; Table 4) or intravenously (0.5 mg/kg; Table 3) were similar (9%–10%). To estimate the extent of absorption, oral bioavailability values were obtained via $F_a = (AUC_{po} * D_{iv} / AUC_{iv} * D_{po})$. Compound (1) displayed moderate-to-high oral bioavailability (Table 4; $F_a = 0.58$). In contrast, we observed metabolism and PK differences when we administered analogs with modifications in the B-ring. There was a statistical difference ($P < 0.0001$) between the IC_{50} values for compound (3) versus (6) in the in vitro hURAT1 assay (Table 1); the methoxy in the 5-benzofuran position was a more potent hURAT1 inhibitor. There was also a statistical difference ($P = 0.0029$; F test, $P = 0.0313$) regarding the extent of Phase I in vitro metabolism (Table 2) where 6-methoxy (3) was metabolized faster than 5-methoxy (6). In contrast to the in vitro samples that produced Phase II metabolites, extracted in vivo blood samples contained low

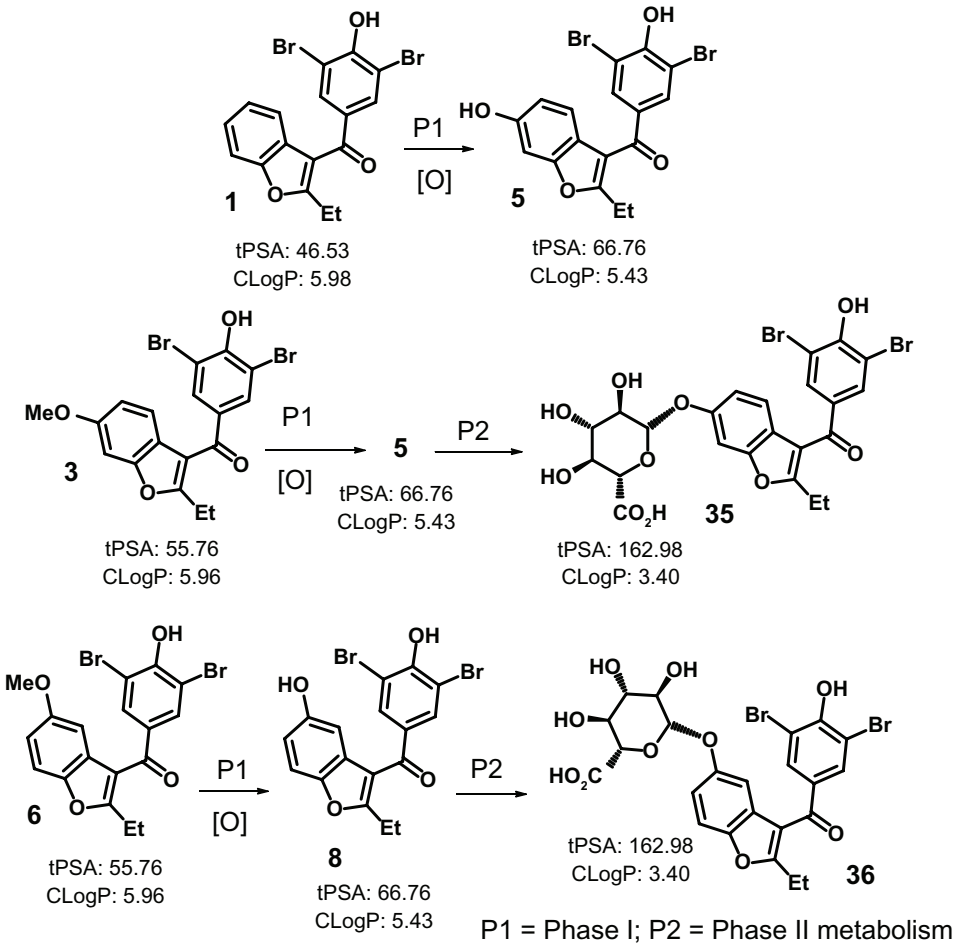

Figure 2 Biotransformation of benzbromarone (1) and analogs (3) and (6).

Table 4 Rat pharmacokinetic summary (n = 4 ± SD)

Oral	Dose mg/kg	T_{max} hours	$T_{1/2}$ hours	C_{max} µg/mL	$AUC_{0-\infty}$ µg · hr/mL	Average F_a
(1)/CMC	16.4	5.0 ± 1.2	6.5 ± 0.7	21.99 ± 6.62	172.92 ± 18.16	0.58
(M) (5)		5.0 ± 2.0	10.7 ± 4.1	1.47 ± 0.30	19.87 ± 8.17	0.59[a]
(3)/CMC	16.3	7.0 ± 1.2	5.9 ± 0.3	3.41 ± 0.86	39.65 ± 10.22	0.13
(M) (5)		7.0 ± 2.0	8.2 ± 0.8	7.67 ± 2.30	108.75 ± 25.06	0.33[a]
(5)/CMC	16.9	4.5 ± 1.0	9.1 ± 1.8	4.42 ± 1.76	51.63 ± 32.79	0.25
(6)/CMC	16.5	6.5 ± 1.9	4.9 ± 0.2	3.13 ± 0.78	27.23 ± 14.91	0.31
(M) (8)		6.7 ± 1.2	9.3 ± 2.6	1.11 ± 0.68	7.39 ± 0.42	0.32[a]
(8)/CMC	15.2	5.0 ± 2.0	8.6 ± 1.5	0.21 ± 0.17	2.12 ± 0.55	0.07
(9)/CMC	17.2	6.5 ± 1.0	5.2 ± 1.3	7.89 ± 2.07	73.66 ± 11.64	0.41[a]
(3)/HBENβCD	16.3	2.8 ± 0.5	10.7 ± 1.4	3.46 ± 0.83	25.25 ± 5.23	0.08
(M) (5)		2.5 ± 0.6	11.5 ± 2.9	9.14 ± 1.89	144.46 ± 43.51	0.38[a]

Note: [a]Estimated bioavailability if one adds parent and active metabolite AUC (AUC parent + AUC metabolite).

Abbreviations: AUC, area under the curve; C_{max}, peak blood concentration; CMC, carboxy-methyl cellulose sodium; F_a, orally absorbed fraction; HBENβCD, hydroxybutenyl-beta-cyclodextrin; M, active metabolite formed from the administered parent compound; SD, standard deviation; $T_{1/2}$, half-life; T_{max}, time after administration to achieve peak blood concentration.

levels of glucuronide. We attribute the Phase II in vitro and in vivo discrepancy to alamethacin, a detergent added to the in vitro incubates, which enhances the accessibility of substrate to enzyme and produces higher quantities of glucuronide.[13,17]

Compared with the parent drug, the amount of active metabolite (5) formed in vivo via (3) accounted for 31% and 73% of the total AUC observed intravenously and orally, respectively. Hence, the oral administration of 5 produced a larger (AUC metabolite/AUC parent) ratio (2.74) than via orbital sinus administration (0.44). In contrast, active metabolite (8) formed in vivo via (6) accounted for 21% of the total AUC regardless of route of administration. These results support the notion that intestinal first-pass metabolism differences between the two methoxy analogs may exist. Therefore, we conducted rat intestine microsomal incubations; (3) and (6) in the presence of NADPH produced CL_{int} data (n = 3 ± SD; 27.3 ± 5.7, and 6.5 ± 1.4 for [3] and [6], respectively) suggesting that in vitro metabolism of (3) via rat intestinal microsomes was statistically faster ($P = 0.0255$) than (6). Hence, gastrointestinal first-pass metabolism appears to be more profound with methoxy analog (5) than with compound (6) (Table 4). Methoxy analog (3) versus (6) revealed no statistical difference between their oral bioavailability F_a values ($P = 0.1283$; F test, $P = 0.0177$) and was also true if one included active metabolites (5) and (8) ($P = 0.5432$; F test, $P = 0.4400$). Comparing the two hydroxyl analogs ([5] versus [8]), there was no statistical difference ($P = 0.3067$; F test, 0.9579) between in vitro hURAT1 assay (Table 1) IC_{50} values. Due to the high variability observed with orally dosed 6-hydroxy (5) (Tables 3 and 4), the differences between the $AUC_{0-\infty}$ and F_a for (5) versus (8) were also not statistically different ($P = 0.0568$; F test, $P < 0.0001$) and ($P = 0.1117$; F test, $P = 0.0064$), respectively. The methoxy analogs (3) and (6), relative to hydroxyl analogs (5) and (8), illustrate that methoxy analogs have an intrinsically higher propensity to be orally absorbed. If one predicts that unionized compounds diffuse across membranes whereas ionized forms do not readily diffuse across membranes, then one may attribute the lower oral bioavailability of di-phenols (5) and (8), relative to mono-phenols (3) and (6), to the additional ionizable group. Although the predicted cLog P (Figure 3) for di-phenol (5) (5.4) was lower than mono-phenol (3) (6.0), phenol (3) can produce a resonance stabilized anion (27), whereas di-phenol (5) can produce two distinct anions, (28) and (29).

We also observed significant differences when we compared the replacement of methoxy (6) or hydroxy (8) with fluoro (9). Compound (9) was metabolized in vitro to an oxidative metabolite (M + 16 amu) consistent with 6-hydroxy-5-fluoro analog. Furthermore, the data (Table 1) illustrate that the replacement of the methoxy or phenol with a fluoro group produced a more potent hURAT1 inhibitor and exhibited good oral bioavailability (Table 4; $F_a = 0.41$). Although formulation development was not a main goal of the current work, we did conduct a preliminary formulation study using cyclodextrin HBenβCD and 6-methoxy analog (3).[12,13] Compared with the oral CMC dose (Table 4), the cyclodextrin formulation did not produce a statistical difference in F_a. However, dissolution rate was clearly influenced with the T_{max} shifting from, essentially, 7 hours to 3 hours (Table 3). Although glucuronidated metabolites (35) and (36) were detectable via liver microsomal incubations, the

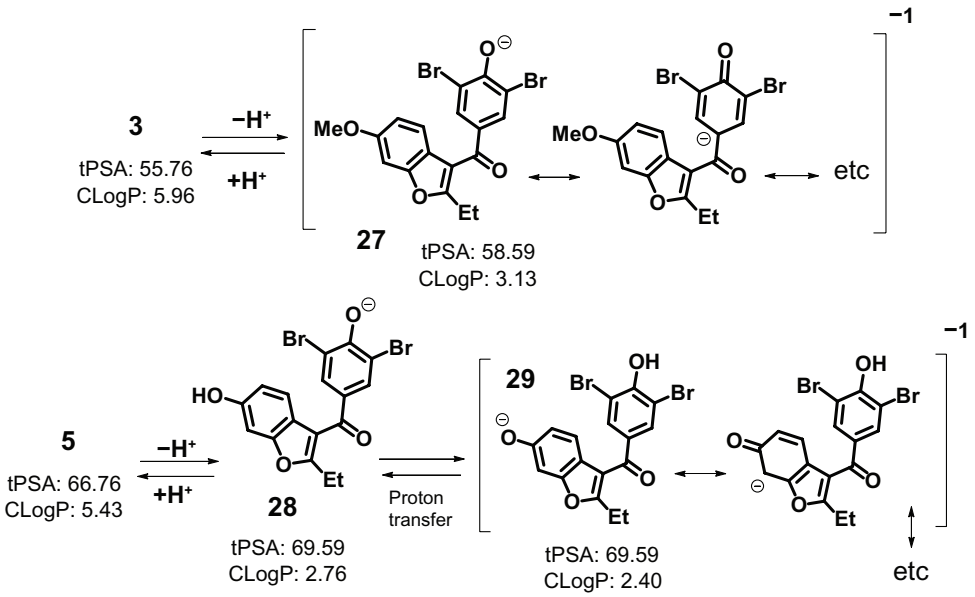

Figure 3 Phenolic dissociation pathways for compounds (3) and (5).

extracted in vivo blood samples did not reveal extensive quantities of the Phase II metabolites. The longer $T_{1/2}$ values observed via the oral dosing (Table 4) may reflect potential entero-hepatic circulation. Therefore, the observation for significant first-pass enterocyte metabolism of analog (3) warrants additional research to explore the formation, stability, transport, and distribution of metabolites (35) and (36).

Conclusion

The current study assessed the metabolism and oral bioavailability of six different hURAT1 inhibitors. The results illustrate that one may successfully prepare potent hURAT1 inhibitors, and that template I molecules exhibit moderate to good oral bioavailability in male Sprague-Dawley rats. As elevated levels of uric acid are known to play a pivotal role in certain human diseases (cardiovascular, chronic renal, diabetes, and hypertension), we believe that the design and development of potent uric acid transport inhibitors may lead to novel therapeutic agents by lowering the level of serum uric acid.

Acknowledgments

The research was funded by J-Pharma Co, Ltd (Tokyo, Japan) and also utilized services of the Medicinal Chemistry Core facility (MFW) housed within the Department of Pharmaceutical Sciences (DOPS), University of Colorado, Anschutz Medical Campus. In part, the MCC has been funded via Colorado Clinical and Translational Sciences Institute Grant 5UL1RR025780 from the National Center for Research Resources at the National Institutes of Health (NCRR/NIH; Bethesda, MA). We also wish to thank Dr Gregory A Hanley at East Tennessee State University for his assistance regarding the orbital sinus dosing.

Disclosure

The authors report no conflicts of interest in this work.

References

1. Adlersberg D, Ellenberg M. Effect of carbohydrate and fat in the diet on uric acid excretion. *J Biol Chem*. 1939;128:379–385.
2. Yu KH, Luo SF, Tsai WP, Huang YY. Intermittent elevation of serum urate and 24-hour urinary uric acid excretion. *Rheumatology*. 2004;43:1541–1545.
3. Enomoto A, Kimura H, Chairoungdua A, et al. Molecular identification of a renal urate anion exchanger that regulates blood urate levels. *Nature*. 2002;417:447–452.
4. Saag KG, Choi H. Epidemiology, risk factors, and lifestyle modifications for gout. *Arthritis Res Ther*. 2006;8(Suppl 1):S2.
5. Cameron JS. Uric acid and renal disease. *NNNA*. 2006;25:1055–1064.
6. Kang DH, Han L, Ouyang X, et al. Uric acid causes vascular smooth muscle cell proliferation by entering cells via a functional urate transporter. *Am J Nephrol*. 2005;25:425–433.
7. Nakagawa T, Hu H, Zharikov S, et al. A causal role for uric acid in fructose-induced metabolic syndrome. *Am J Physiol Renal Physiol*. 2006;290:F625–F631.
8. Price KL, Sautin YY, Long DA, et al. Human vascular smooth muscle cells express a urate transporter. *J Am Soc Nephrol*. 2006;17:1791–1795.
9. Anzai N, Jutabha P, Endou H. Renal solute transporters and their relevance to serum urate disorder. *Curr Hypertens Rev*. 2010;6:148–154.
10. Wempe MF, Jutabha P, Quade B, et al. Developing potent human uric acid transporter 1 (hURAT1) inhibitors. *J Med Chem*. 2011;54:2701–2713.
11. Wempe MF, Quade B, Jutabha P, et al. Human uric acid transporter 1 (hURAT1): an inhibitor structure-activity relationship (SAR) study. *Nucleosides Nucleotides Nucleic Acids*. 2011;30:1312–1323.

12. Wempe MF, Buchanan CM, Buchanan NL, et al. Pharmacokinetics of letrozole in male and female rats: influence of complexation of hydroxybutenyl-β-cyclodextrin. *J Pharm Pharmacol*. 2007;59:795–802.
13. Wempe MF, Wacher VJ, Ruble KM, et al. Pharmacokinetics of raloxifene in male Wistar-Hannover rats: influence of complexation with hydroxybutenyl-β-cyclodextrin. *Int J Pharm*. 2008;346:25–37.
14. Obach RS. Prediction of human clearance of twenty-nine drugs from hepatic microsomal intrinsic clearance data: an examination of in vitro half-life approach and nonspecific binding to microsomes. *Drug Metab Dispos*. 1999;27:1350–1359.
15. March J. *Advanced Organic Chemistry: Reactions, Mechanisms, and Structure.* New York, NY: John Wiley & Sons; 1992:26–74.
16. Wempe MF, Rice PJ, Lightner JW, et al. Metabolism and pharmacokinetic studies of JPH203, an L-amino acid transporter 1 (LAT1) selective compound. *Drug Metab Pharmacokinet*. 2012;27:155–161.
17. Little JA, Lehman PA, Nowell S, Samokyszyn V, Radominska A. Glucuronidation of all-trans-retinoic acid and 5,6-epoxy-all-trans-retinoic acid: activation of rat liver microsomal UDP-glucuronosoyltransferase activity by alamethicin. *Drug Metab Dispos*. 1997;25:5–11.

Supplementary materials

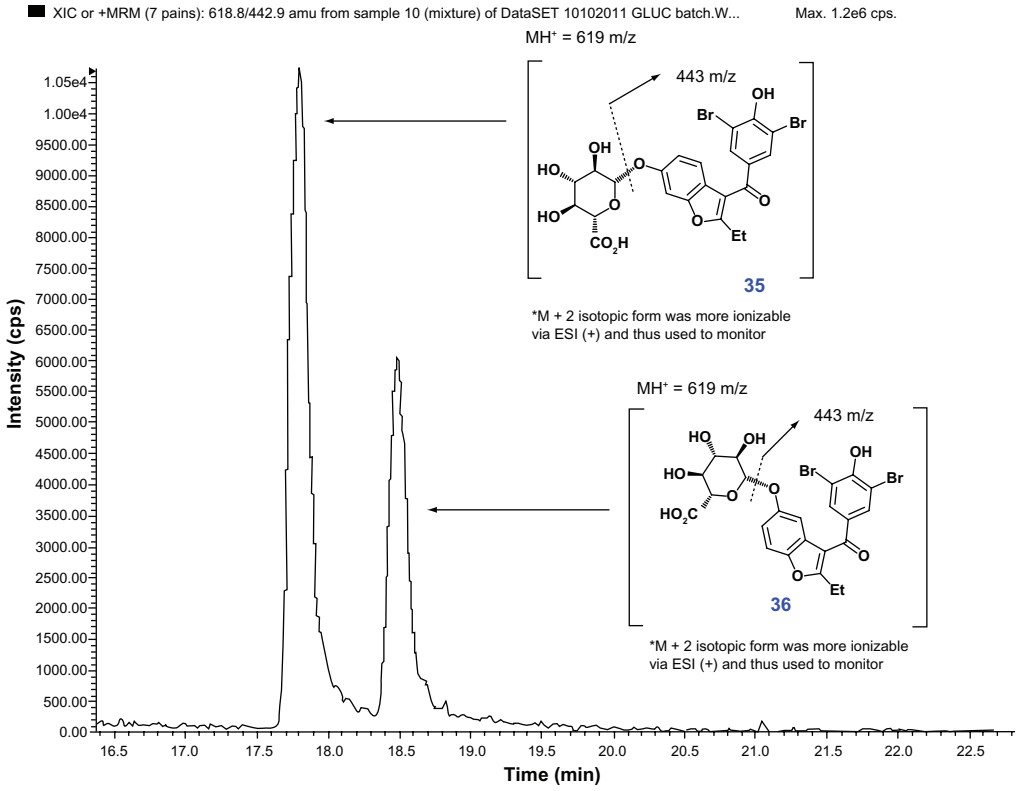

Figure S1 Extracted ion chromatogram; 619 → 443 m/z.

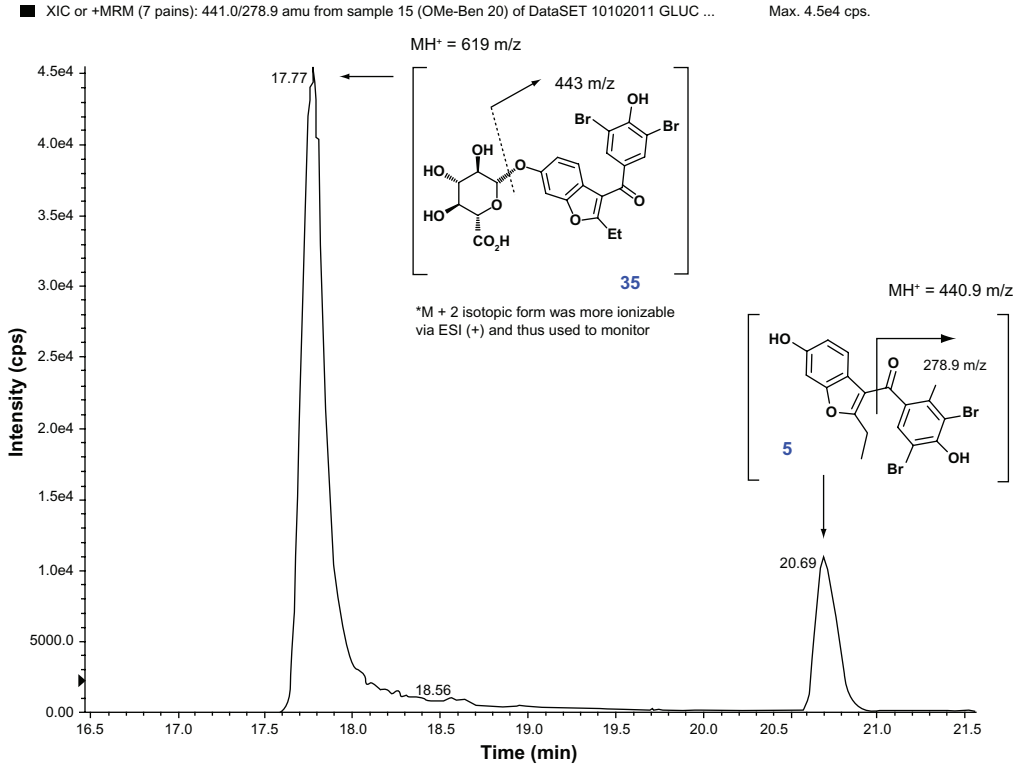

Figure S2 Compound (5) to glucuronide (35); rat liver microsomal incubate of (3).

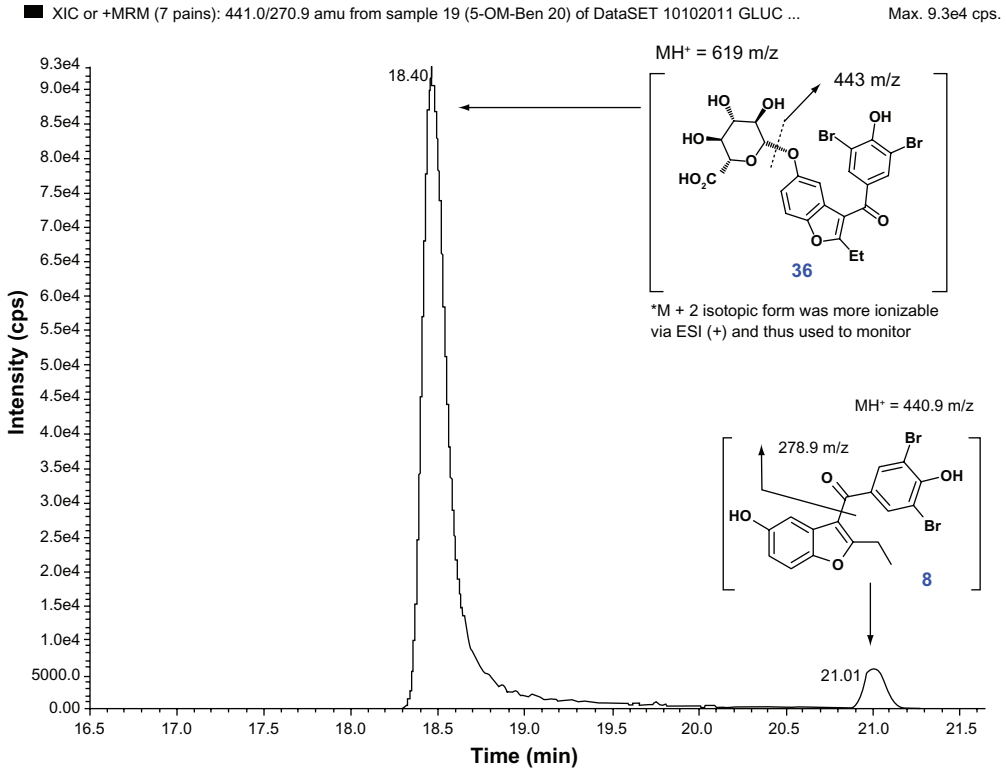

Figure S3 Compound (8) to glucuronide (36); rat liver microsomal incubate of (6).

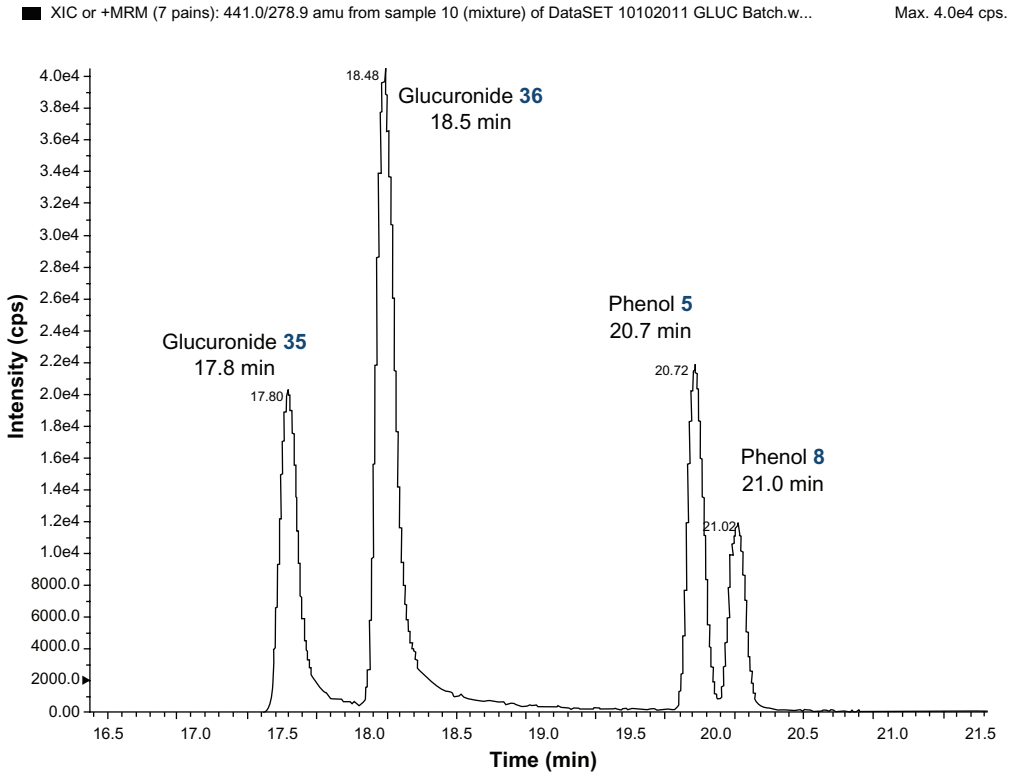

Figure S4 All four illustrating baseline separations of (5), (8), (35), and (36).

Notes: Agilent Technologies, Zorbax extended-C18 250 × 4.6 mm, 5 micron column at 40°C with a flow rate of 0.4 mL/min was used. The mobile phase consisted of A: 10 mM (NH_4OAc), 0.1% formic acid in H_2O, and B: 50:50 ACN:MeOH. The chromatography method used was 95% A for 3.0 min, ramped to 95% B at 16.00 minutes and held for 7.5 minutes, and, lastly, brought back to 95% A at 26.5 minutes and held for 4.5 minutes (31.0 minutes total run time).

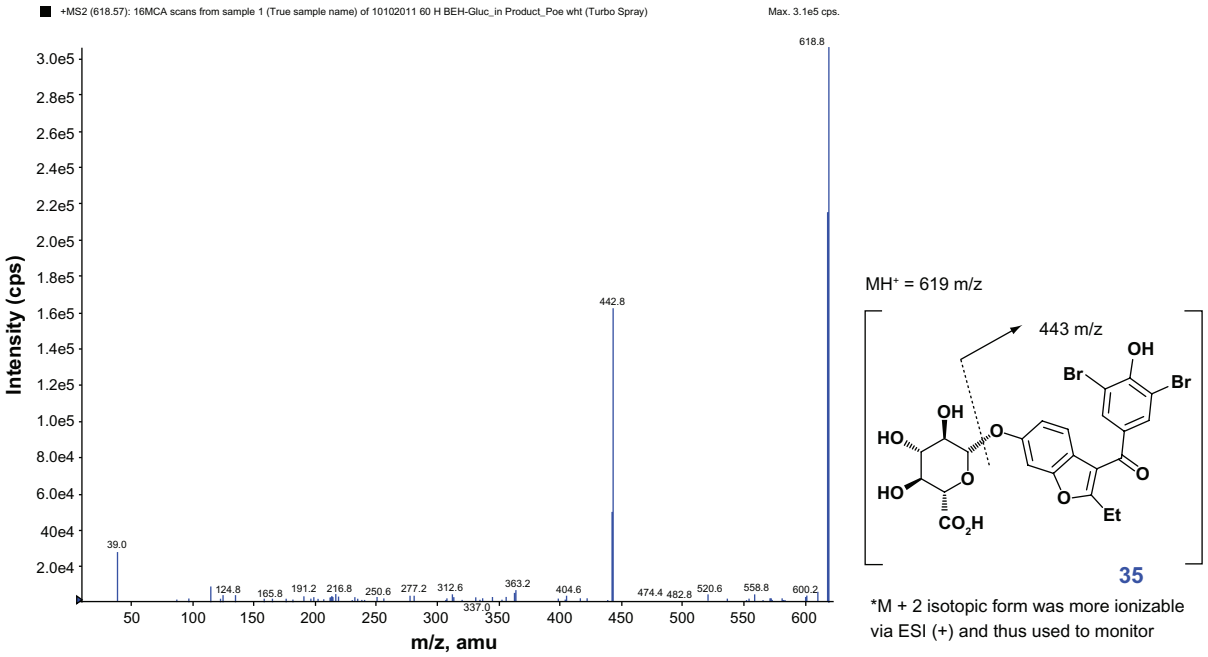

Figure S5 Electro-spray ionization (ESI) (+) mode mass spectrometric fragmentation of glucuronide (35).

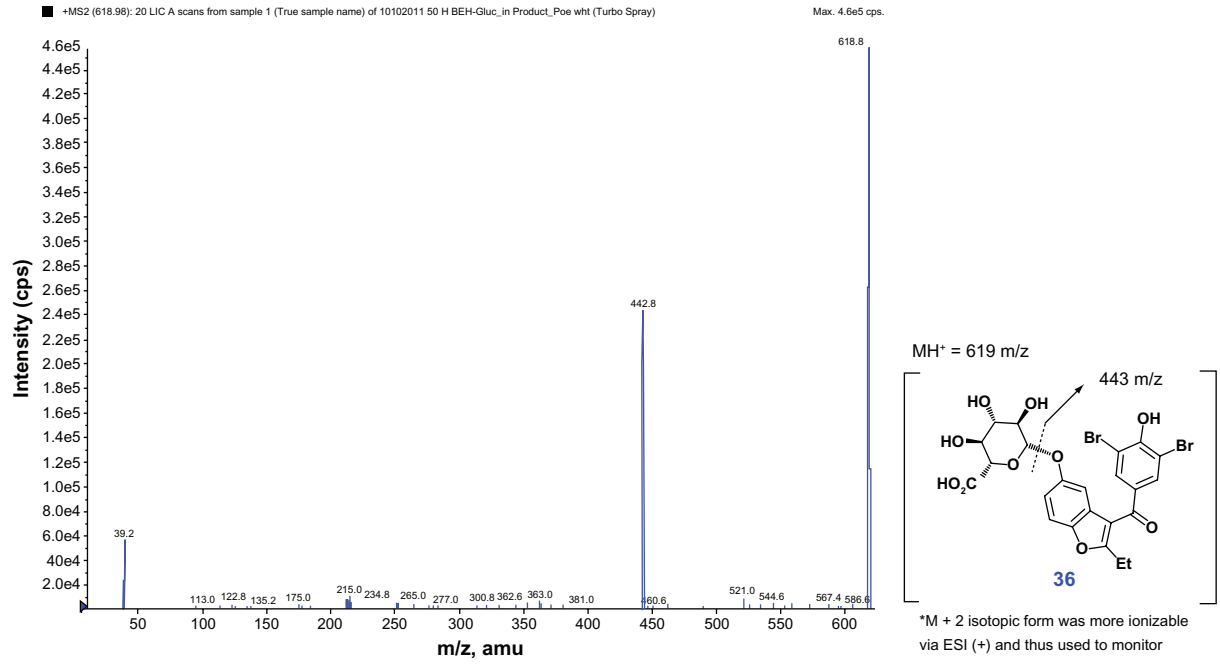

Figure S6 Electro-spray ionization (ESI) (+) mode mass spectrometric fragmentation of glucuronide (36).